







RESEARCH ARTICLE | JANUARY 18 2023

# Magneto-thermal conductivity effect and enhanced thermoelectric figure of merit in $\text{Ag}_2\text{Te}$

Keisuke Hirata  ; Kentaro Kuga ; Masaharu Matsunami ; Minyue Zhu; Joseph P. Heremans ; Tsunehiro Takeuchi 

 Check for updates

*AIP Advances* 13, 015016 (2023)

<https://doi.org/10.1063/5.0131326>

 CHORUS



## APL Energy

### Latest Articles Online!

**Read Now**



# Magneto-thermal conductivity effect and enhanced thermoelectric figure of merit in $\text{Ag}_2\text{Te}$

Cite as: AIP Advances 13, 015016 (2023); doi: 10.1063/5.0131326

Submitted: 19 October 2022 • Accepted: 23 December 2022 •

Published Online: 18 January 2023



View Online



Export Citation



CrossMark

Keisuke Hirata,<sup>1,a)</sup>  Kentaro Kuga,<sup>1</sup>  Masaharu Matsunami,<sup>1</sup>  Minyue Zhu,<sup>2</sup> Joseph P. Heremans,<sup>2,3,4</sup>  and Tsunehiro Takeuchi<sup>1,5,6,7</sup> 

## AFFILIATIONS

<sup>1</sup>Toyota Technological Institute, Nagoya, Aichi 468-8511, Japan

<sup>2</sup>Department of Mechanical and Aerospace Engineering, The Ohio State University, Columbus, Ohio 43210, USA

<sup>3</sup>Department of Material Science and Engineering, The Ohio State University, Columbus, Ohio 43210, USA

<sup>4</sup>Department of Physics, The Ohio State University, Columbus, Ohio 43210, USA

<sup>5</sup>Research Center for Smart Energy Technology of Toyota Technological Institute, Nagoya, Aichi 468-8511, Japan

<sup>6</sup>CREST, Japan Science and Technology Agency, Tokyo 102-0076, Japan

<sup>7</sup>MIRAI, Japan Science and Technology Agency, Kawaguchi, Saitama 332-0012, Japan

<sup>a)</sup> Author to whom correspondence should be addressed: [kei.h.research@gmail.com](mailto:kei.h.research@gmail.com)

## ABSTRACT

In this study, we report a large magneto-thermal conductivity effect, potentially usable in heat flow switches and thermoelectric devices, in  $\text{Ag}_2\text{Te}$  over a wide temperature range, including room temperature. When a magnetic field of  $\mu_0 H = 9$  T is applied to  $\text{Ag}_2\text{Te}$  at 300 K along the direction perpendicular to the heat and electric currents, the thermal conductivity  $\kappa$  decreases by a remarkable 61%. This effect is mainly caused by the suppressed electronic thermal conductivity in association with a significant magnetoresistance effect, but the suppression of the thermal conductivity is larger than that of the electrical conductivity, presumably due to a field-induced decrease in the Lorenz ratio. Its very low lattice thermal conductivity, as low as  $0.5 \text{ W m}^{-1} \text{ K}^{-1}$ , also greatly contributes to the large relative magneto-thermal conductivity effect. The significant decrease in thermal conductivity and the 18% increase in the Seebeck coefficient  $S$  lead to a nearly 100% increase in the thermoelectric figure of merit  $zT = S^2 \sigma T \kappa^{-1}$  despite the 43% decrease in electrical conductivity  $\sigma$ .

© 2023 Author(s). All article content, except where otherwise noted, is licensed under a Creative Commons Attribution (CC BY) license (<http://creativecommons.org/licenses/by/4.0/>). <https://doi.org/10.1063/5.0131326>

## INTRODUCTION

Heat flow switches<sup>1-3</sup> control the magnitude of heat flow through a device by external triggers; thermal diodes<sup>1,4-7</sup> allow heat to flow in only one direction; waste heat is directly converted into useful electric energy in thermoelectric devices.<sup>8,9</sup> These heat management devices, particularly if they are to be realized as all-solid-state devices operable over a large temperature range, would be very useful for converting abundant waste heat into useful energy to realize a carbon-neutral, sustainable society.

The performance of heat management devices generally depends on the thermal conductivity of the constituent materials.

For instance, the performance of a heat flow switch is usually based on the variation in thermal conductivity by external triggers, and this variation needs to be maximized. There are thermal diodes made from two materials with a thermal conductivity that is significantly temperature dependent; their thermal rectification ratio then depends on the strength of this dependence.<sup>6</sup> It is also well known that the conversion efficiency of a thermoelectric device is generally improved by decreasing the thermal conductivity.

To create a significant variation in the thermal conductivity of solid materials, we need to control the electronic conduction and/or that of other collective excitations, such as lattice vibrations, magnons, spinons, polarons, etc. Several techniques to control the

thermal conductivity of solid materials were demonstrated using external parameters:<sup>1,7</sup> temperature, electric field, magnetic field, pressure, and light. However, the development of practical devices and materials to control the heat flow remains a major challenge because of the small variation ratio, complicated structure, slow switching, narrow operating temperature range, and degradation upon cycling.

Here, we focus on an all-solid-state thermal conductivity controlling technique using a magnetoresistance (MR) effect characterized by robustness, remote operation, fast switching, non-degradation, and easy implementation. The MR effect is the variation in electrical resistivity ( $\rho$ ) owing to an applied magnetic field ( $H$ ), defined as  $MR = [\rho(H) - \rho(0)]/\rho(0)$ .

From the Boltzmann transport equation in the linear response regime, the electronic part of thermal conductivity ( $\kappa_{\text{ele}}$ ) under open-circuit conditions is written as<sup>10</sup>

$$\kappa_{\text{ele}} = \frac{1}{e^2 T} \int_{-\infty}^{\infty} \sigma(\varepsilon, T) (\varepsilon - \mu)^2 \left( -\frac{\partial f_{\text{FD}}}{\partial \varepsilon} \right) d\varepsilon - S^2 \sigma T, \quad (1)$$

$$\sigma = \int_{-\infty}^{\infty} \sigma(\varepsilon, T) \left( -\frac{\partial f_{\text{FD}}}{\partial \varepsilon} \right) d\varepsilon, \quad (2)$$

$$S = -\frac{1}{|e|T} \frac{\int_{-\infty}^{\infty} \sigma(\varepsilon, T) (\varepsilon - \mu) \left( -\frac{\partial f_{\text{FD}}}{\partial \varepsilon} \right) d\varepsilon}{\int_{-\infty}^{\infty} \sigma(\varepsilon, T) \left( -\frac{\partial f_{\text{FD}}}{\partial \varepsilon} \right) d\varepsilon}. \quad (3)$$

Here,  $e$ ,  $\varepsilon$ ,  $\mu$ ,  $\sigma$ ,  $S$ ,  $T$ , and  $f_{\text{FD}}$  represent the elementary charge of an electron, energy, chemical potential, electrical conductivity, Seebeck coefficient, absolute temperature, and Fermi-Dirac distribution function, respectively. The  $\sigma(\varepsilon, T)$  included in the integral of Eqs. (1)–(3) is so called “spectral conductivity,” indicating the contribution of electronic states designated by  $\varepsilon$  to the electrical conductivity. In an isotropic electronic structure,  $\sigma(\varepsilon, T)$  is written as

$$\sigma(\varepsilon, T) = \frac{e^2}{3} D(\varepsilon) v_g^2(\varepsilon) \tau(\varepsilon, T). \quad (4)$$

Here,  $D(\varepsilon)$ ,  $v_g(\varepsilon)$ , and  $\tau(\varepsilon, T)$  are the energy-dependent density of states, group velocity, and relaxation time of the electron. The integrand in Eqs. (1)–(3) consists of the same  $\sigma(\varepsilon, T)$  and different window functions,  $W_n = (\varepsilon - \mu)^n (-\partial f_{\text{FD}}/\partial \varepsilon)$ , which determine the energy range of electrons that contribute to  $\kappa_{\text{ele}}$ ,  $\sigma$ , and  $S$ ,<sup>10</sup> as shown in Fig. S1 in the [supplementary material](#).

When the spectral conductivity is a linear function of energy, by using the second-order Bethe–Sommerfeld expansion, the 1st-term of Eq. (1) becomes  $L_0 \sigma T$ , where  $L_0 = \pi^2 k_B^2 / (3e^2) = 2.44 \times 10^{-8} \text{ V}^2 \text{ K}^{-2}$  is known as the Sommerfeld value of the Lorentz ratio.<sup>10</sup> At that time, the absolute value of  $S$  should become negligibly small, satisfying  $L_0 \gg S^2$ . As a result, Eq. (1) is approximated by  $\kappa_{\text{ele}} = L_0 \sigma T$ , which is widely known as the Wiedemann–Franz (WF) law generally observable in metals.

Thus, through the spectral conductivity, the MR effect is capable of inducing a nontrivial variation in thermal conductivity to become one of the origins of magneto-thermal conductivity (MTC) effects, defined as  $MTC = [\kappa(H) - \kappa(0)]/\kappa(0)$ .

Most prior research for the MTC effect induced by the MR effect was carried out at low temperatures. At very low temperatures below 10 K, a large carrier mobility and a small lattice thermal conductivity are simultaneously realized as the necessities for a larger MTC effect, but these characteristics become less significant at high temperatures, including 300 K. For example, the largest MTC effect of about  $-100000\%$  was reported in  $\text{PtSn}_4$  at 2 K with  $\mu_0 H = 9 \text{ T}$ .<sup>11</sup> Recently, around room temperature, a giant magnetoresistance (GMR) device<sup>12</sup> was reported to show an MTC effect of about  $+100\%$ , and single crystals of Bi–Sb alloys<sup>13</sup> and  $\text{Cd}_3\text{As}_2$ <sup>14</sup> were also reported to show MTC effects of about  $-60\%$ . However, materials/devices showing a large MTC effect around room temperature are still presently limited.

This situation indicates that once we find a material showing a remarkable MTC effect near room temperature, the material would be a new candidate as the constituent material in heat flow switches and thermoelectric devices for waste heat management.

The total thermal conductivity ( $\kappa_{\text{total}}$ ) of solids is generally represented by the sum of the contributions from electrons ( $\kappa_{\text{ele}}$ ) and lattice vibrations ( $\kappa_{\text{lat}}$ ). A material possessing a large MR effect with a high electrical conductivity is favorable for observing a large variation in  $\kappa_{\text{ele}}(H)$ . Note also here that  $\kappa_{\text{lat}}$  does not generally vary with the magnetic field, except for several specific materials and conditions.<sup>15–17</sup> Therefore, the variation in  $\kappa_{\text{total}}$ , defined as a switch ratio (SR) between open ( $H = 0$ ) and closed ( $H \neq 0$ ) conductances, is written by Eq. (5) as a function of  $H$ . It is naturally understood from Eq. (5) that a very low  $\kappa_{\text{lat}}$  is of crucial importance for obtaining a large MTC effect,

$$SR = \frac{\kappa_{\text{total}}(H)}{\kappa_{\text{total}}(H = 0)} = \frac{\kappa_{\text{ele}}(H) + \kappa_{\text{lat}}}{\kappa_{\text{ele}}(H = 0) + \kappa_{\text{lat}}}. \quad (5)$$

By searching the material simultaneously possessing a large MR effect and a low  $\kappa_{\text{lat}}$ , we found  $\text{Ag}_2\text{Te}$  as one of the most favorable candidates to obtain a large MTC effect around room temperature.  $\text{Ag}_2\text{Te}$  undergoes a structural phase transition at around 420 K; the low-temperature phase is a non-magnetic semiconductor possessing a narrow bandgap (a few tens of meV) and a monoclinic crystal structure.<sup>18–20</sup> Importantly,  $\text{Ag}_2\text{Te}$  was reported to show a large linear transverse MR effect of more than  $+100\%$  under 300 K and  $\mu_0 H = 4 \text{ T}$ <sup>21</sup> with no signs of saturation up to  $\mu_0 H = 60 \text{ T}$ ,<sup>22</sup> a moderately high electrical conductivity of  $1000\text{--}2000 \text{ S cm}^{-1}$ ,<sup>4,21</sup> corresponding to  $\kappa_{\text{ele}} = L_0 \sigma T = 0.73\text{--}1.5 \text{ W m}^{-1} \text{ K}^{-1}$ , and an extremely low lattice thermal conductivity of  $0.3\text{--}0.5 \text{ W m}^{-1} \text{ K}^{-1}$ .<sup>23,24</sup> Thus, we predicted that a substantial MTC effect should be observable in  $\text{Ag}_2\text{Te}$  around room temperature. Besides, the sign of the transverse magneto-Seebeck effect in  $\text{Ag}_2\text{Te}$  was reported to depend on temperatures, whereas that of the MR effect was positive regardless of temperature.<sup>25</sup> Therefore, it is also worth investigating the temperature and magnetic field dependences of the thermoelectric figure of merit ( $zT = S^2 \sigma T \kappa^{-1}$ ).

For investigating the transverse magneto-effect on the thermoelectric properties of  $\text{Ag}_2\text{Te}$ , we measured the magnetic field dependence and the temperature dependence of the thermal conductivity, electrical conductivity, and Seebeck coefficient. As a result, we report, in this paper, a remarkable MTC effect of  $-61\%$  and a significant increase in  $zT$  of  $\sim 100\%$  at 300 K by changing  $\mu_0 H$  from 0 to 9 T.

## EXPERIMENTAL PROCEDURE

Bulk samples were prepared by a self-propagating high-temperature synthesis (SHS) method, which enables us to quickly, easily, and accurately synthesize  $\text{Ag}_2\text{Te}$ , known as a line compound.<sup>26</sup> The details of the SHS method were reported in our previous study.<sup>4</sup> For performing accurate physical property measurements, we densified the SHS-synthesized  $\text{Ag}_2\text{Te}$  samples by pressing them in a cylindrical die at  $\sim 673$  K for 15 min under a uniaxial pressure of 50 MPa. We confirmed from the Archimedes method that the finally obtained polycrystalline bulks possessed 99% of theoretical density.

The phases involved in the samples were identified by crystal structure analysis based on synchrotron radiation x-ray powder diffraction (SR-XRPD), which allows us to perform Rietveld analysis for the refinement of crystal parameters. In the SR-XRPD measurements, the sample was packed in a borosilicate capillary ( $\phi 0.19$  mm in inner diameter) and measured by a transmission method in a Debye-Scherrer geometry with a 25 keV light source at BL02B2 in the SPring-8 synchrotron radiation facility (Hyogo, Japan).<sup>27</sup> The programs of RIETAN-FP<sup>28</sup> and VESTA<sup>29</sup> were used for the Rietveld analysis.

The chemical composition was also analyzed by using an electron-probe micro-analyzer (EPMA) (JEOL's JXA-8230) and a scanning electron microscope equipped with energy-dispersive x-ray spectroscopy (SEM-EDX) (SU6600, Hitachi). The acceleration voltage was 20 keV both in EPMA and SEM-EDX measurements.

The temperature (10–300 K) and magnetic field dependences ( $\mu_0 H = 0 - \pm 9$  T) of thermal conductivity, electrical conductivity, and Seebeck coefficient were measured with the Thermal Transport Option (TTO)<sup>30</sup> in the Physical Property Measurement System (PPMS) manufactured by Quantum Design, Inc. The experimental setup for the TTO is presented in Fig. 1. The sample was prepared in a cylindrical shape of  $\phi 6.0$  mm diameter and 3.1 mm length, which is recommended in the TTO manual to be a favorable thermal conductance with radiative heat loss mitigated in materials possessing  $\kappa < 1.5$   $\text{W m}^{-1} \text{K}^{-1}$ . Two gold-coated copper disks, attached to both sides of the sample by silver epoxy (H20E, EPO-TEK), were used as an electric current lead and heat spreader. The MR

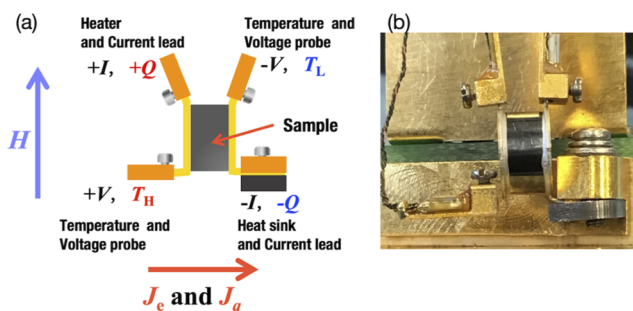


**FIG. 1.** (a) Schematic and (b) photograph of the PPMS-TTO setup for measuring thermal conductivity, electrical conductivity, and the Seebeck coefficient under magnetic field ( $H$ ) perpendicular to heat ( $J_q$ ) and electric currents ( $J_e$ ). The labels of  $\pm I$ ,  $\pm V$ ,  $T_{H,L}$ , and  $\pm Q$  represent the current leads, voltage probes, temperature probes, and heater/heat sink, respectively.

effect of the metal disks was confirmed to be negligibly small in the [supplementary material](#). The temperature and voltage probe shown in Fig. 1 consisted of a thermometer (Cernox1050, Lake Shore) and a manganin wire. The measurement error of the thermometer, arising from the applied magnetic field, was reported to be 0.002%–0.4% in the temperature and magnetic field ranges of this study.<sup>31</sup> This error is much smaller than the MTC effect of  $\text{Ag}_2\text{Te}$  observed in this study and could be safely ignored. The heat-relaxation and the AC method with the setup shown in Fig. 1 enabled us to measure the thermal conductivity, electrical conductivity, and Seebeck coefficient with the same setup. The temperature difference between the hot and cold sides of the sample was 1%–4% of the environmental temperature for thermal conductivity and Seebeck measurement, and the excitation electric current was 0.1–10 mA (1 Hz) for electrical conductivity measurement. Convective and radiative heat losses from the sample were mitigated by a vacuum level of  $\sim 10^{-4}$  Torr and a gold-coated copper isothermal shield, respectively. The error of TTO measurement was analyzed in the [supplementary material](#).

By using a bar-shaped sample, the electrical conductivity was measured with a homemade four-probe setup for accurately determining the zero-field data, and the Hall resistivity was also measured up to  $\mu_0 H = \pm 9$  T with the horizontal rotator option in the PPMS for estimating the carrier concentration.

The carrier concentration dependence of magneto-effects on thermoelectric properties was also investigated under  $\mu_0 H = 0 - \pm 1$  T at 105, 200, and 300 K by using a six-probe setup under a steady-state condition in a Janis cryostat (Lake Shore Cryotronics). The details of the experimental setup and measurement method are described in Fig. S3 of the [supplementary material](#). The carrier concentration was tuned by adding extra Ag/Te to almost stoichiometric  $\text{Ag}_2\text{Te}$  before sintering to become  $\text{Ag}_{2\pm\delta}\text{Te}$ , in which excess Ag provides electrons and excess Te provides holes.<sup>32</sup>

## RESULTS

Figures 2(a) and 2(b) show the SR-XRPD pattern of  $\text{Ag}_2\text{Te}$  and the crystal structure of  $\text{Ag}_2\text{Te}$  constructed from refined parameters from the Rietveld analysis, respectively. Although the line compound nature of  $\text{Ag}_2\text{Te}$  easily leads to the formation of impurity phases even with a very tiny compositional shift, we confirmed that all the observed diffraction peaks were identified as those from the monoclinic structure (space group:  $P2_1/c$ ; Pearson symbol:  $mP12$ ) phase of  $\text{Ag}_2\text{Te}$ . The Rietveld refinement using the SR-XRPD pattern revealed that the splitting of Ag-sites [Fig. 2(b)] led to better reliability factors than those in the no split-site model, as shown in Tables S1 and S2 of the [supplementary material](#). Then, we considered that the splitting of Ag-sites induced a strong anharmonic oscillation to realize the extremely low  $\kappa_{\text{lat}}$  of  $\text{Ag}_2\text{Te}$ .

From the SEM-EDX (Fig. 3) and the EPMA (Table S3 in the [supplementary material](#)) measurements, we also confirmed that our sample possessed uniform element distribution, no voids/cracks, and an almost stoichiometric composition. These characteristics allowed us to accurately determine the physical properties.

Figure 4 summarizes the magnetic field dependence of the (a) thermal conductivity, (b) electrical conductivity, (c) Seebeck coefficient, (d) power factor ( $PF = S^2\sigma$ ), and (e)  $zT$  of  $\text{Ag}_2\text{Te}$  at 300 K. The minor asymmetry observable in the data is ascribable to the

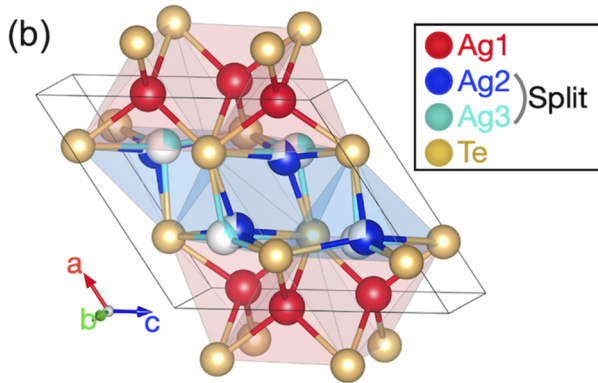
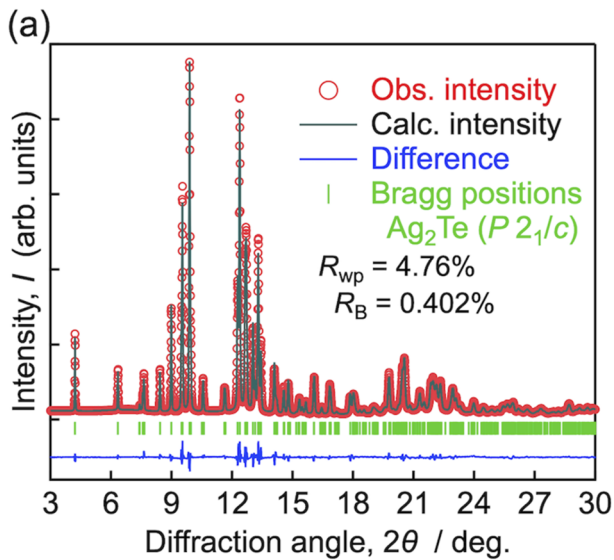


**FIG. 2.** (a) Powder XRD pattern and Rietveld refinement of  $\text{Ag}_2\text{Te}$  at 300 K using 25 keV synchrotron radiation. Reliability factors based on the weighted profile and Bragg intensities are denoted as  $R_{\text{wp}}$  and  $R_{\text{B}}$ , respectively. (b) Schematic of the refined crystal structure of  $\text{Ag}_2\text{Te}$  (space group:  $P2_1/c$ ; Pearson symbol:  $mP12$ ) drawn by VESTA.<sup>29</sup> The lattice constants of  $\text{Ag}_2\text{Te}$  were estimated to be  $a = 8.0658 \text{ \AA}$ ,  $b = 4.4739 \text{ \AA}$ ,  $c = 8.9720 \text{ \AA}$ , and  $\beta = 123.14^\circ$ . The details of crystal parameters are shown in Table S2 in the [supplementary material](#).

magnetic field and heat/electric current not being perfectly perpendicular in the Fig. 1 setup. By changing  $\mu_0 H$  from 0 to 9 T, we successfully observed a remarkable MTC effect of  $-61\%$  from  $1.7$  to  $0.66 \text{ W m}^{-1} \text{ K}^{-1}$ , which is the largest value as a single phase polycrystalline material at room temperature.

The electrical conductivity decreased by  $43\%$  ( $MR = 75\%$ ), from  $1156 \text{ S cm}^{-1}$  at 0 T to  $661 \text{ S cm}^{-1}$  at 9 T. The inset of Fig. 4(b) displays the squared magnetic field dependence of the symmetrized MR effect, in which the MR effect possessed quadratic behavior at low fields and quasi-linear behavior at high fields. This behavior was also reported in a prior study for  $\text{Ag}_2\text{Te}$ .<sup>35</sup>

The Seebeck coefficient systematically increased by  $18\%$ , indicating variation of electronic structure around the chemical

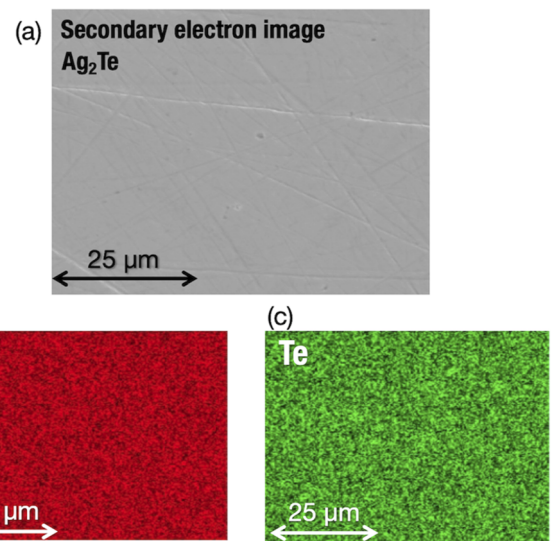


**FIG. 3.** SEM-EDX observation on  $\text{Ag}_2\text{Te}$ : (a) secondary electron image and (b) and (c) element distribution maps for Ag and Te.

potential. This magneto-Seebeck effect partly counteracted the MR effect, leading to a relatively small decrease in the  $PF$  by  $20\%$ .

Mainly due to the large MTC effect, the  $zT$  increased by  $\sim 100\%$ , from  $0.16$  to  $0.32$ . A higher magnetic field of more than  $\mu_0 H = 9 \text{ T}$  would not lead to a larger MTC effect and  $zT$  because the electrical conductivity keeps decreasing with increasing magnetic field whereas the thermal conductivity and the Seebeck coefficient are almost saturated above  $\mu_0 H = 6 \text{ T}$ .

The magnetic field dependence of Hall resistivity ( $\rho_{\text{H}}$ ) is also shown in the inset of Fig. 4(b). The negative sign of Hall resistivity indicates that electrons behave as the majority carrier. This is consistent with that expected from the sign of the Seebeck coefficient. Since the Hall resistivity clearly showed linear dependence with the magnetic field, we estimated the carrier density,  $n$ , by using the single band model of  $n = 1/(|R_{\text{H}}|e)$ <sup>34</sup> to be  $1.7 \times 10^{18} \text{ cm}^{-3}$  at 300 K.

To clarify  $\kappa_{\text{lat}}$  and  $\kappa_{\text{ele}}$  contributions to the MTC effect of  $\text{Ag}_2\text{Te}$ , first, we measured the magnetic field dependence of the thermal conductivity in polycrystalline  $\text{Ag}_2\text{S}$ , possessing the same crystal structure (space group:  $P2_1/c$ ; Pearson symbol:  $mP12$ ) with  $\text{Ag}_2\text{Te}$  but a much smaller electrical conductivity of  $\sim 10^{-9} \text{ S cm}^{-1}$  at 300 K with 1 eV bandgap.<sup>35</sup> As shown in Fig. 4(a), the  $\text{Ag}_2\text{S}$  had no MTC effect; therefore, we considered that the  $\kappa_{\text{lat}}$  of  $\text{Ag}_2\text{Te}$  was also independent of the magnetic field.

Then, we fitted the magnetic-field-dependent thermal conductivity of  $\text{Ag}_2\text{Te}$  using an equation assuming that the sum of a constant  $\kappa_{\text{lat}}$  and a variable  $\kappa_{\text{ele}}$  consisting of linear and quadratic MR effects. From the fitting, the  $\kappa_{\text{lat}}$  of  $\text{Ag}_2\text{Te}$  was estimated to be  $0.50 \text{ W m}^{-1} \text{ K}^{-1}$ . Furthermore, the magnetic susceptibility of  $\text{Ag}_2\text{Te}$  showed only a very weak diamagnetism (see Fig. S4 in the [supplementary material](#)), suggesting no magnon contribution to the MTC effect in  $\text{Ag}_2\text{Te}$ . Thus, we identified that the marked MTC effect in  $\text{Ag}_2\text{Te}$  resulted from the synergy of the suppressed  $\kappa_{\text{ele}}$  owing to the MR effect and the very low  $\kappa_{\text{lat}}$  of  $\sim 0.5 \text{ W m}^{-1} \text{ K}^{-1}$ .

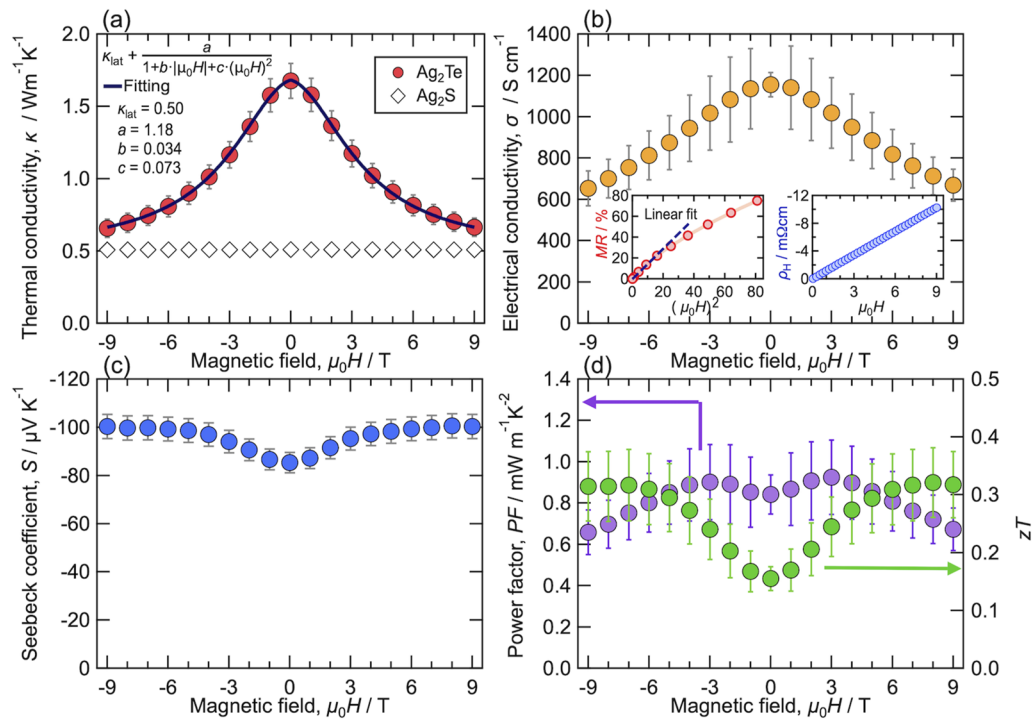


**FIG. 4.** Magnetic field dependence of (a) thermal conductivity, (b) electrical conductivity, (c) the Seebeck coefficient, (d) PF, and (d)  $zT$  in  $\text{Ag}_2\text{Te}$  at 300 K. In Fig. 4(a), the thermal conductivity of  $\text{Ag}_2\text{Te}$  was fitted using an equation by assuming that a constant  $\kappa_{\text{lat}}$  and a variable  $\kappa_{\text{ele}}$  consisting of linear and quadratic MR effects. The left and right insets of Fig. 4(b) show the squared magnetic field dependence of symmetrized MR effect and the magnetic field dependence of Hall resistivity ( $\rho_H$ ), respectively.

It should be worthwhile to note here that the 61% decrease in the thermal conductivity owing to the magnetic field was certainly larger than the 43% reduction in the electrical conductivity. This experimentally revealed fact indicates that the WF law is invalid for explaining the magnetic field dependence of the MTC effect in  $\text{Ag}_2\text{Te}$ . The interpretations of this phenomenon are addressed in the discussion part.

Figure 5 summarizes the temperature dependence of the (a) thermal conductivity, (b) electrical conductivity, (c) Seebeck coefficient, and (d)  $zT$  of  $\text{Ag}_2\text{Te}$  at  $\mu_0 H = 0$  T and 9 T. The temperature-dependent behaviors of the electrical conductivities with and without the magnetic field agree with those of previously reported for n-type  $\text{Ag}_2\text{Te}$ .<sup>21</sup> Besides, radiative heat loss was confirmed to have a minor effect on the measured thermal conductivity, as shown in Fig. S5 in the [supplementary material](#).

To analyze the temperature dependence of the MTC effect, we roughly estimated  $\kappa_{\text{ele}}$  by tentatively using the WF law with the Sommerfeld value and  $\kappa_{\text{lat}}$  by subtracting the  $\kappa_{\text{ele}}$  from the measured  $\kappa_{\text{total}}$  in the zero-field data. This process assumes that  $\kappa_{\text{lat}}$  does not depend on the magnetic field, which holds as long as the temperature is not near the peak in thermal conductivity,<sup>15</sup> which is at 17 K here. As shown in Fig. 5(a), the estimated  $\kappa_{\text{lat}}$  dominated the total thermal conductivity below 40 K, resulting in the same thermal conductivity regardless of the magnitude of the magnetic field. The  $\kappa_{\text{lat}}$  decreased with increasing temperature above 20 K by the getting intensified Umklapp scattering, whereas the  $\kappa_{\text{ele}}$  increased owing to

the coefficient of  $T$  in the WF law and the slightly increased electrical conductivity. Therefore, the MTC effect of  $\text{Ag}_2\text{Te}$  developed with increasing temperature above 40 K and became obvious at high temperatures to show the maximum value at 300 K in the measured range. Besides, the inconsistency in the  $\kappa_{\text{lat}}$  between Figs. 5(a) and 4(a) implies that the use of the WF law with  $L_0$  is not appropriate. This is discussed later.

The Seebeck coefficients with and without the magnetic field show different temperature dependence in the temperature range from 50 to 300 K. This fact suggests that the applied magnetic field leads to a nontrivial variation in the electronic structure over the wide temperature range. The increase in the absolute value of the Seebeck coefficient by the magnetic field was observed above 230 K. Consequently, we found that the enhancement of  $zT$  by the magnetic field was obtainable above 200 K and that the  $zT$  in our measured range became maximum at 300 K.

To find a condition leading to a large magneto-effect on thermal and electrical conductivities, we also investigated the carrier concentration dependence of  $[\sigma(\mu_0 H = 1 \text{ T}) - \sigma(0)]$  and  $[\kappa(\mu_0 H = 1 \text{ T}) - \kappa(0)]$ , as shown in Fig. 6. The data obtained from Fig. S3 setup unfortunately included non-negligible radiation heat loss owing to the very low thermal conductivity of  $\text{Ag}_2\text{Te}$  and sample geometry effect; thus, we evaluated the magneto-effect not by the ratio but by the difference in value. Besides, the difference in the experimental setup and conditions between Figs. S3 and 1 probably led to a difference in the obtained data.

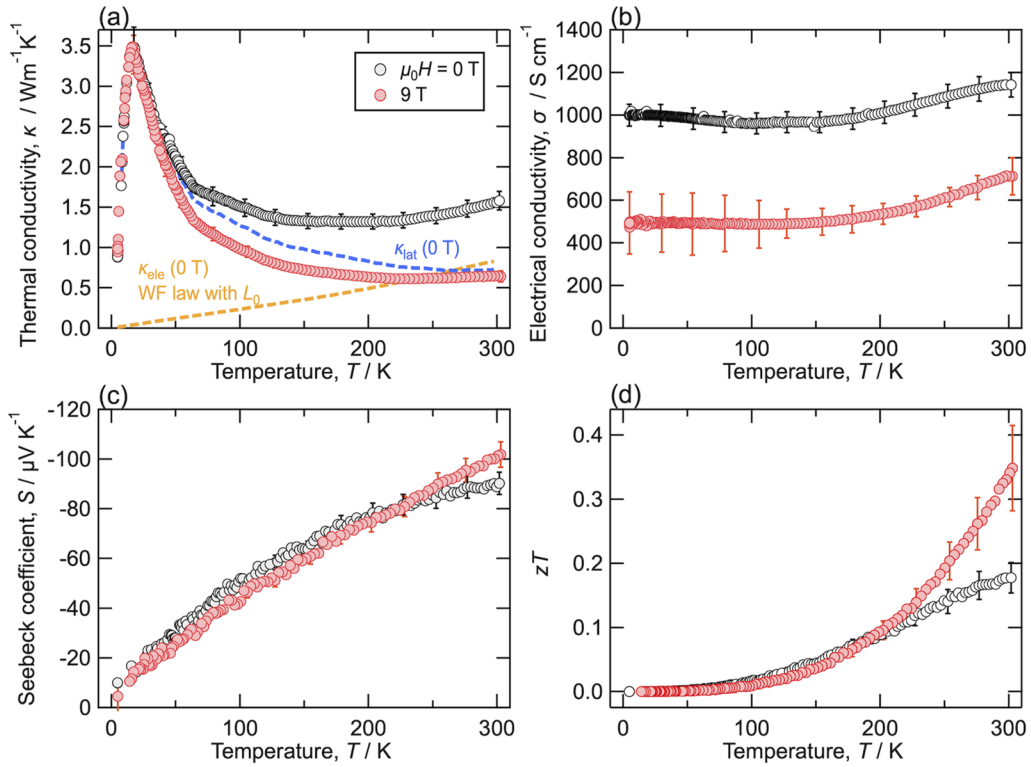


**FIG. 5.** Temperature dependence of (a) thermal conductivity, (b) electrical conductivity, (c) the Seebeck coefficient, and (d)  $zT$  in  $\text{Ag}_2\text{Te}$  at a magnetic field of  $\mu_0H = 0$  and 9 T. From the thermal electrical conductivities at zero field, the electronic thermal conductivity ( $\kappa_{\text{ele}}$ ) was roughly estimated by tentatively using the Wiedemann–Franz law with a Lorentz ratio of  $2.44 \times 10^{-8} \text{ V}^2 \text{ K}^{-2}$ , and the lattice thermal conductivity ( $\kappa_{\text{lat}}$ ) was deduced by subtracting the estimated  $\kappa_{\text{ele}}$  from the measured thermal conductivity.

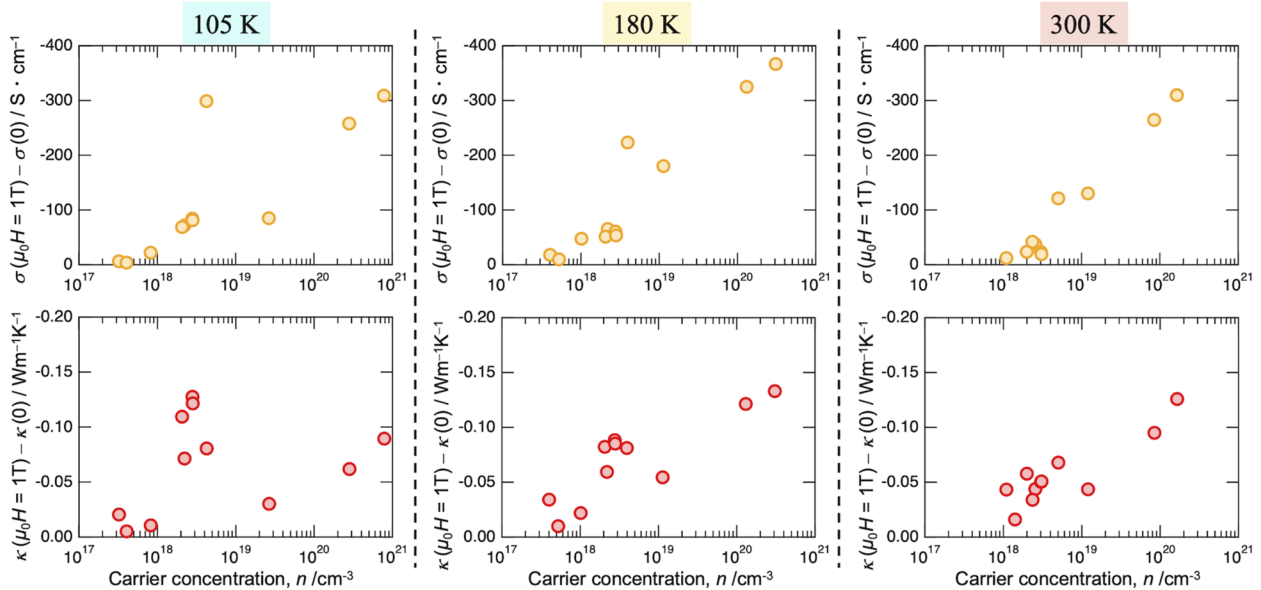


**FIG. 6.** Carrier concentration dependence of the magnetic field effect on electrical and thermal conductivities, evaluated by  $[\sigma(\mu_0H = 1 \text{ T}) - \sigma(0)]$  and  $[\kappa(\mu_0H = 1 \text{ T}) - \kappa(0)]$ , respectively. The plotted data were obtained with the setup of Fig. S3.

As shown in Fig. 6, we found a trend that the changes in thermal and electrical conductivities induced by the magnetic field increased with increasing carrier concentration. This characteristic is usable when the magnitude of changes has more priority than the ratio of changes, although the magnitude of thermal conductivity increases with increasing carrier concentration.

Besides, the carrier concentration dependences of magneto-effects on the Seebeck coefficient and the  $zT$  are shown in Fig. S6 of the supplementary material, and we found that an increase in the  $zT$  owing to magnetic field was obtainable in low carrier concentration region.

## DISCUSSIONS

As shown in Figs. 4(a) and 4(b), the decrease ratio of  $\kappa$  due to the magnetic field became larger than that of  $\sigma$  despite the absence of magnetic-field-dependent phonon and magnon contribution to the thermal conductivity. This experimental fact indicates that the magnetic field dependence of the thermal conductivity in  $\text{Ag}_2\text{Te}$  is not describable using the WF law; therefore, we need to consider the fine energy dependence of spectral conductivity around the chemical potential, which is out of the prerequisites of the WF law, and also magnetic field effect on it. As in Eqs. (6) and (7), let us define the Lorentz ratio,  $L$ , and the ratio of integrating the same spectral conductivity by the different window functions,  $W_2$  and  $W_0$ , as  $L_1$ ,

$$\kappa_{\text{ele}} = L\sigma T = (L_1 - S^2)\sigma T, \quad (6)$$

$$L_1 = \frac{1}{(eT)^2} \frac{\int_{-\infty}^{\infty} \sigma(\varepsilon, T)(\varepsilon - \mu)^2 \left(-\frac{\partial f_{\text{FD}}}{\partial \varepsilon}\right) d\varepsilon}{\int_{-\infty}^{\infty} \sigma(\varepsilon, T) \left(-\frac{\partial f_{\text{FD}}}{\partial \varepsilon}\right) d\varepsilon}. \quad (7)$$

This definition of  $L_1$  enables us to infer the shape of the spectral conductivity by comparing  $L_1$  and  $L_0$  because  $L_1 = L_0$  is obtainable from Eq. (7) only when the spectral conductivity around the chemical potential is a linear function of energy.<sup>10</sup> By assuming  $\kappa_{\text{lat}} = 0.50 \text{ W m}^{-1} \text{ K}^{-1}$  from our fitting result in Fig. 4(a), we estimated  $\kappa_{\text{ele}}$  by subtracting the  $\kappa_{\text{lat}}$  from the  $\kappa_{\text{total}}$  and then calculated  $L_1$  from Eq. (6), although these contain uncertainties from the  $\kappa_{\text{lat}}$ . The calculated  $L_1$  changes from  $4.1 \times 10^{-8} \text{ V}^2 \text{ K}^{-2}$  at zero-field to  $1.8 \times 10^{-8} \text{ V}^2 \text{ K}^{-2}$  at  $\mu_0 H = 9 \text{ T}$ . These values were used in the following discussion. As a reference, the  $L$  was estimated to be  $3.4 \times 10^{-8} \text{ V}^2 \text{ K}^{-2}$  at zero field and  $0.80 \times 10^{-8} \text{ V}^2 \text{ K}^{-2}$  at  $\mu_0 H = 9 \text{ T}$ .

So far, several physical origins have been proposed for the MR effect in  $\text{Ag}_2\text{Te}$ , and the observation that the Lorentz ratio decreases with field may shed new experimental light on the problem. The proposed models involve (1) Landau bands formation with gapless linear dispersion in the quantum limit induced by the slight off-stoichiometry of  $\text{Ag}$ ,<sup>36</sup> (2) the electronic structure of topological insulators,<sup>20,37</sup> and (3) electric current distortion due to  $\text{Ag}$ -impurity.<sup>38,39</sup> Although the discussion for the origin remains inconclusive, we considered the latter two as plausible interpretations for the MTC effect in  $\text{Ag}_2\text{Te}$ , namely, interpretations based on the electronic structure effect and the current distortion effect. This is discussed next.

In the case of the electronic structure effect, we need to consider the variation in the shape of energy-dependent spectral conductivity

induced by the magnetic field. From Eq. (7) and Fig. S1,  $L_1 > L_0$  can be obtained when the spectral conductivity within about  $\pm 10k_{\text{B}}T$  from the chemical potential becomes concave. The observed  $L_1 > L_0$  at zero-field, therefore, implies that the spectral conductivity in  $\text{Ag}_2\text{Te}$ , reported as a narrow-gap semiconductor with a few tens of meV bandgap<sup>19</sup> and as a topological insulator candidate,<sup>20</sup> is concave. This concave is presumably obtainable from its density of states and/or relaxation time. For example, pseudo-gap materials<sup>10</sup> and narrow/zero-gap semiconductors,<sup>40-43</sup> possessing concave density of states, are reported to have bipolar thermal diffusion effect, which is considered as one of the reasons for a larger  $L$  than  $L_0$ . On the other hand, in a topological insulator, the selective scattering mechanism of carriers is capable of introducing a strong energy dependence on the relaxation time around the bulk band edge,<sup>44</sup> it can also lead to concave spectral conductivity depending on the position of the chemical potential. Conversely,  $L_1 < L_0$  results from convex spectral conductivity. Since we observe the decrease of the  $L_1$  with the field, this implies that the spectral conductivity becomes more convex presumably due to variations in the relaxation time and/or the density of states with the field. The former hypothesis is consistent with other results. Lee *et al.*<sup>45</sup> showed how bringing the chemical potential closer to the band intersection led to a larger MR effect, i.e., a larger reduction in relaxation time. Therefore, when the chemical potential is located slightly apart from the band intersection, the electrons contributing to  $\kappa_{\text{ele}}$  mainly existing at  $\varepsilon = \mu \pm 2.4k_{\text{B}}T$  might possess a shorter relaxation time than those contributing to  $\sigma$  mainly existing at  $\varepsilon = \mu$  under the same magnetic field, leading to convex spectral conductivity. As for the latter, the convex also might be realized by Landau bands formation in the quantum limit, in which only the lowest band contains electrons, proposed by Abrikosov<sup>36</sup> for the explanation of linear transverse MR effect in  $\text{Ag}_2\text{Te}$  and Bi.

In the case of the current distortion effect, a large difference in carrier mobility between randomly distributed metallic Ag-impurities and the semiconducting  $\text{Ag}_2\text{Te}$  matrix was reported to generate electric current distortion under magnetic field, leading to positive linear transverse MR effect. Besides, the electric current distortion known as the geometrical MR effect might also exist in a setup such as that shown in Fig. 1. If this scenario is true, the MTC effect of  $\text{Ag}_2\text{Te}$  is not ascribable to the variation in the material's electrical conductivity, and heat current distortion effect, such as the Righi-Ledeuc effect,<sup>46</sup> might be one of the reasons for the larger reduction in  $\kappa$  than  $\sigma$  under the same magnetic field.

Quantitative analyses and simulations based on the above-mentioned interpretations would provide important knowledge about the MTC effect to readers but are very challenging. Therefore, leaving these analyses as a topic in another paper, we decided to emphasize here only that our strategy, employing  $\text{Ag}_2\text{Te}$  characterized by the very low  $\kappa_{\text{lat}}$  and large MR effect, enables us to observe the remarkable MTC effect even at room temperature.

The fact that the MTC is much larger than the MR should be favorable in practical applications. In addition, a required magnetic field should be as low as the commercial neodymium magnet of  $\mu_0 H = 1 \text{ T}$ <sup>47</sup> for practical applications. Finally, we comment on the possible strategies to make the MTC effect of  $\text{Ag}_2\text{Te}$  more practical, as shown below.

The low value of  $\kappa_{\text{lat}}$  contributes to the enhancement of the MTC effect, as is seen from Eq. (5). At room temperature, the  $\kappa_{\text{lat}}$



of  $0.50 \text{ W m}^{-1} \text{ K}^{-1}$  in  $\text{Ag}_2\text{Te}$  is almost the lowest class among dense solids. For instance, the mean free path of phonons ( $l$ ) was estimated to be shorter than the lattice constant,  $3.8 \text{ \AA}$ , using the gas model of  $\kappa_{\text{lat}} = \frac{1}{3} C \cdot v \cdot l$ :  $C = 84.8 \text{ J mol}^{-1} \text{ K}^{-1}$  is the reported heat capacity.<sup>5</sup>  $v = 1933 \text{ m s}^{-1}$  is the mean phonon group velocity deduced by our pulse-echo ultrasound measurement. Therefore, nano-structuring should be ineffective in reducing  $\kappa_{\text{lat}}$  further. Element substitution leading to a heavier average mass and weaker atomic bonding is the preferred way to further reduce  $\kappa_{\text{lat}}$ .

Another strategy is to increase the variation of  $\kappa_{\text{ele}}$  and decrease the required magnetic field at that time. These are obtainable by understanding the origin of the MR and MTC effect in  $\text{Ag}_2\text{Te}$ . How this would work depends on which explanation underlies the MR.

In the case that the electronic structure effect underpins the MR, precise transport measurement and high-resolution angle-resolved photoemission spectroscopy using a single crystal would enable us to investigate the spectral conductivity for the detailed analyses of the Lorentz ratio, MR, and MTC. For example, a larger MR effect of above 100% at  $4 \text{ T}^{21}$  was reported in  $\text{Ag}_{2+\delta}\text{Te}$  ( $\delta \sim 10^{-4}$ ) with a carrier density of  $\sim 6.3 \times 10^{18} \text{ cm}^{-3}$  at 300 K. Therefore, understanding its electronic structure would allow us to find out the condition leading to a larger MTC effect with a smaller required magnetic field.

In the case that the current distortion effect underpins the MR, first, the existence of heat current distortion in  $\text{Ag}_2\text{Te}$  should be proved by investigating the Righi-Ledeuc effect. Then, we would be able to explore the technique of how to increase the MTC effect and decrease the required magnetic field by using element substitution, composite effect, geometrical designing of the material and experimental setup, etc.

## CONCLUSION

For obtaining a large magneto-thermal conductivity (MTC) effect even around room temperature, we focused, in this study, on  $\text{Ag}_2\text{Te}$  characterized by a large magnetoresistance (MR) effect, a high electrical conductivity, and a low lattice thermal conductivity. The thermoelectric properties of  $\text{Ag}_2\text{Te}$  were investigated in the temperature range from 10 to 300 K and magnetic fields of up to  $\mu_0 H = \pm 9 \text{ T}$ . The MTC effect increased with increasing temperature and became the maximum value of  $-61\%$  at 300 K with 9 T. This effect was mainly caused by the synergy of a suppressed electronic thermal conductivity associated with a MR effect of  $+75\%$  and an extremely low lattice thermal conductivity of  $\sim 0.5 \text{ W m}^{-1} \text{ K}^{-1}$  related to a strong anharmonic oscillation induced by the Ag-site splitting. Besides, the Seebeck coefficient was increased by 18% under the influence of the magnetic field. Consequently, the thermoelectric figure of merit was increased to 0.32, which is twice as large as the zero-field value. Our findings and strategies proposed to magnify the effects would facilitate the utilization of the MTC effect in all-solid-state heat flow switches and thermoelectric devices working around room temperature.

## SUPPLEMENTARY MATERIAL

See the [supplementary material](#) for details of the shape of window functions in Eqs. (1)–(3), the magnetoresistance of gold-coated

copper disks used in the setup of Fig. 1, the error analysis of PPMS-TTO measurement, the experimental setup and method using the Janis cryostat, the refined crystal parameters by the Rietveld analyses, the quantitative composition analysis by the EPMA, the magnetic susceptibility measurement by VSM, the radiative heat loss analysis of PPMS-TTO measurement, and carrier concentration dependence of the magneto-effect on thermoelectric properties.

## ACKNOWLEDGMENTS

This work was supported by JSPS KAKENHI, Japan, through Grant No. 21J15714. J.P.H. was supported by the U.S. Office of Naval Research MURI Program, through Grant No. N00014-21-1-2377. M.Z. was supported by the U.S. National Science Foundation MRSEC Program, through Grant No. DMR 201 1876. The synchrotron radiation XRD experiments were performed at the BL02B2 of SPring-8 with the approval of the Japan Synchrotron Radiation Research Institute (JASRI) (Proposal No. 2021B1837). The authors would like to thank Dr. S. Kawaguchi and N. Kubo for their assistance during the experiments at SPring-8 and the experiments using PPMS-TTO, respectively.

## AUTHOR DECLARATIONS

### Conflict of Interest

The authors have no conflicts to disclose.

### Author Contributions

**Keisuke Hirata:** Conceptualization (lead); Data curation (lead); Formal analysis (lead); Funding acquisition (lead); Investigation (lead); Project administration (lead); Resources (equal); Validation (lead); Visualization (lead); Writing – original draft (lead); Writing – review & editing (lead). **Kentarō Kuga:** Investigation (supporting); Writing – review & editing (supporting). **Masaharu Matsunami:** Supervision (supporting); Writing – review & editing (supporting). **Minyue Zhu:** Investigation (supporting); Writing – review & editing (supporting). **Joseph P. Heremans:** Conceptualization (equal); Resources (lead); Supervision (equal); Writing – review & editing (equal). **Tsunehiro Takeuchi:** Conceptualization (equal); Funding acquisition (supporting); Project administration (equal); Resources (lead); Supervision (lead); Writing – review & editing (equal).

## DATA AVAILABILITY

The data that support the findings of this study are available from the corresponding author upon reasonable request.

## REFERENCES

- G. Wehmeyer, T. Yabuki, C. Monachon, J. Wu, and C. Dames, *Appl. Phys. Rev.* **4**, 041304 (2017).
- T. Matsunaga, K. Hirata, S. Singh, M. Matsunami, and T. Takeuchi, *Mater. Trans.* **62**, 16 (2021).
- K. Hirata, T. Matsunaga, S. Singh, M. Matsunami, and T. Takeuchi, *Jpn. J. Appl. Phys.* **60**, 124004 (2021).
- K. Hirata, T. Matsunaga, S. Saurabh, M. Matsunami, and T. Takeuchi, *Mater. Trans.* **61**, 2402 (2020).
- K. Hirata, T. Matsunaga, S. Singh, M. Matsunami, and T. Takeuchi, *J. Electron. Mater.* **49**, 2895 (2020).

- <sup>6</sup>M. Peyrard, *Europhys. Lett.* **76**, 49 (2006).
- <sup>7</sup>T. Swoboda, K. Klinar, A. S. Yalamarthy, A. Kitanovski, and M. Muñoz Rojo, *Adv. Electron. Mater.* **7**, 2000625 (2021).
- <sup>8</sup>G. J. Snyder and E. S. Toberer, *Nat. Mater.* **7**, 105 (2008).
- <sup>9</sup>S. Singh, K. Hirata, D. Byeon, T. Matsunaga, O. Muthusamy, S. Ghodke, M. Adachi, Y. Yamamoto, M. Matsunami, and T. Takeuchi, *J. Electron. Mater.* **49**, 2846 (2020).
- <sup>10</sup>T. Takeuchi, *Materials, Preparation, and Characterization in Thermoelectrics*, edited by D. M. Rowe (CRC Press, 2012), Chap. 7.
- <sup>11</sup>C. Fu, S. N. Guin, T. Scaffidi, Y. Sun, R. Saha, S. J. Watzman, A. K. Srivastava, G. Li, W. Schnelle, S. S. P. Parkin, C. Felser, and J. Gooth, *Research* **2020**, 1.
- <sup>12</sup>H. Nakayama, B. Xu, S. Iwamoto, K. Yamamoto, R. Iguchi, A. Miura, T. Hirai, Y. Miura, Y. Sakuraba, J. Shiomi, and K. Uchida, *Appl. Phys. Lett.* **118**, 042409 (2021).
- <sup>13</sup>D. Vu, W. Zhang, C. Şahin, M. E. Flatté, N. Trivedi, and J. P. Heremans, *Nat. Mater.* **20**, 1525 (2021).
- <sup>14</sup>J. Xiang, S. Hu, M. Lyu, W. Zhu, C. Ma, Z. Chen, F. Steglich, G. Chen, and P. Sun, *Sci. China: Phys., Mech. Astron.* **63**, 237011 (2020).
- <sup>15</sup>H. Jin, O. D. Restrepo, N. Antolin, S. R. Boona, W. Windl, R. C. Myers, and J. P. Heremans, *Nat. Mater.* **14**, 601 (2015).
- <sup>16</sup>C. Strohm, G. L. J. A. Rikken, and P. Wyder, *Phys. Rev. Lett.* **95**, 155901 (2005).
- <sup>17</sup>K. Sugii, M. Shimosawa, D. Watanabe, Y. Suzuki, M. Halim, M. Kimata, Y. Matsumoto, S. Nakatsuji, and M. Yamashita, *Phys. Rev. Lett.* **118**, 145902 (2017).
- <sup>18</sup>A. van der Lee and J. L. de Boer, *Acta Crystallogr., Sect. C: Cryst. Struct. Commun.* **49**, 1444 (1993).
- <sup>19</sup>T.-T. Yeh, W. H. Lin, W.-Y. Tzeng, P. H. Le, C.-W. Luo, and T. I. Milenov, *J. Alloys Compd.* **725**, 433 (2017).
- <sup>20</sup>A. Sulaev, P. Ren, B. Xia, Q. H. Lin, T. Yu, C. Qiu, S.-Y. Zhang, M.-Y. Han, Z. P. Li, W. G. Zhu, Q. Wu, Y. P. Feng, L. Shen, S.-Q. Shen, and L. Wang, *AIP Adv.* **3**, 032123 (2013).
- <sup>21</sup>R. Xu, A. Husmann, T. F. Rosenbaum, M.-L. Saboungi, J. E. Enderby, and P. B. Littlewood, *Nature* **390**, 57 (1997).
- <sup>22</sup>A. Husmann, J. B. Betts, G. S. Boebinger, A. Migliori, T. F. Rosenbaum, and M.-L. Saboungi, *Nature* **417**, 421 (2002).
- <sup>23</sup>D.-y. Jung, K. Kurosaki, Y. Ohishi, H. Muta, and S. Yamanaka, *Mater. Trans.* **53**, 1216 (2012).
- <sup>24</sup>Y. Pei, N. A. Heinz, and G. J. Snyder, *J. Mater. Chem.* **21**, 18256 (2011).
- <sup>25</sup>Y. Sun, M. B. Salamon, M. Lee, and T. F. Rosenbaum, *Appl. Phys. Lett.* **82**, 1440 (2003).
- <sup>26</sup>K. Zhao, H. Duan, N. Raghavendra, P. Qiu, Y. Zeng, W. Zhang, J. Yang, X. Shi, and L. Chen, *Adv. Mater.* **29**, 1701148 (2017).
- <sup>27</sup>S. Kawaguchi, M. Takemoto, K. Osaka, E. Nishibori, C. Moriyoshi, Y. Kubota, Y. Kuroiwa, and K. Sugimoto, *Rev. Sci. Instrum.* **88**, 085111 (2017).
- <sup>28</sup>F. Izumi and K. Momma, *Solid State Phenom.* **130**, 15 (2007).
- <sup>29</sup>K. Momma and F. Izumi, *J. Appl. Crystallogr.* **44**, 1272 (2011).
- <sup>30</sup>N. R. Dilley, R. C. Black, L. Montes, A. Wilson, and M. B. Simmonds, *MRS Proc.* **691**, G3.5 (2001).
- <sup>31</sup>B. L. Brandt, D. W. Liu, and L. G. Rubin, *Rev. Sci. Instrum.* **70**, 104 (1999).
- <sup>32</sup>H. S. Schnyders, M.-L. Saboungi, and T. F. Rosenbaum, *Appl. Phys. Lett.* **76**, 1710 (2000).
- <sup>33</sup>Y. Zhao, W. Yang, H. S. Schnyders, A. Husmann, G. Zhang, Y. Ren, D. L. Price, H.-K. Mao, and M.-L. Saboungi, *Phys. Rev. B* **98**, 205126 (2018).
- <sup>34</sup>N. W. Ashcroft and N. D. Mermin, *Solid State Physics* (Brooks Cole, Belmont, MA, 1976).
- <sup>35</sup>R. Zamiri, H. Abbastabar Ahangar, A. Zakaria, G. Zamiri, M. Shabani, B. Singh, and J. M. F. Ferreira, *Chem. Cent. J.* **9**, 28 (2015).
- <sup>36</sup>A. A. Abrikosov, *J. Phys. A: Math. Gen.* **36**, 9119 (2003).
- <sup>37</sup>P. Leng, F. Chen, X. Cao, Y. Wang, C. Huang, X. Sun, Y. Yang, J. Zhou, X. Xie, Z. Li, E. Zhang, L. Ai, Y. Yang, and F. Xiu, *Nano Lett.* **20**, 7004 (2020).
- <sup>38</sup>M. M. Parish and P. B. Littlewood, *Nature* **426**, 162 (2003).
- <sup>39</sup>J. Hu, M. M. Parish, and T. F. Rosenbaum, *Phys. Rev. B* **75**, 214203 (2007).
- <sup>40</sup>X. Wang, V. Askarpour, J. Maassen, and M. Lundstrom, *J. Appl. Phys.* **123**, 055104 (2018).
- <sup>41</sup>Z. Luo, J. Tian, S. Huang, M. Srinivasan, J. Maassen, Y. P. Chen, and X. Xu, *ACS Nano* **12**, 1120 (2018).
- <sup>42</sup>J. S. Rhyee, E. Cho, K. Ahn, K. H. Lee, and S. M. Lee, *Appl. Phys. Lett.* **97**, 2010 (2010).
- <sup>43</sup>H. Yoshino and K. Murata, *J. Phys. Soc. Jpn.* **84**, 024601 (2015).
- <sup>44</sup>Y. V. Ivanov, A. T. Burkov, and D. A. Pshenay-Severin, *Phys. Status Solidi B* **255**, 1800020 (2018).
- <sup>45</sup>M. Lee, T. F. Rosenbaum, M.-L. Saboungi, and H. S. Schnyders, *Phys. Rev. Lett.* **88**, 066602 (2002).
- <sup>46</sup>R. T. Delves, *Rep. Prog. Phys.* **28**, 308 (1965).
- <sup>47</sup>P. G. Shewane, M. Gite, and A. Singh, *Int. J. Recent Innov. Trends Comput. Commun.* **2**, 4056 (2014).